Two-dimensional transition metal dichalcogenides under electron irradiation: defect production and doping

Hannu-Pekka Komsa[1], Jani Kotakoski[1,2], Simon Kurasch[3],
Ossi Lehtinen[1], Ute Kaiser[3], and Arkady V. Krasheninnikov[1,4]
[1] *Department of Physics, University of Helsinki, P.O. Box 43, 00014 Helsinki, Finland*
[2] *Department of Physics, University of Vienna, Boltzmanngasse 5, 1190 Wien, Austria*
[3] *Central Facility for Electron Microscopy, Group of Electron Microscopy of Materials Science, University of Ulm, 89081 Ulm, Germany and*
[4] *Department of Applied Physics, Aalto University, P.O. Box 11100, 00076 Aalto, Finland*
(Dated: June 21, 2012)

Using first-principles atomistic simulations, we study the response of atomically-thin layers of transition metal dichalcogenides (TMDs) – a new class of two-dimensional inorganic materials with unique electronic properties – to electron irradiation. We calculate displacement threshold energies for atoms in 21 different compounds and estimate the corresponding electron energies required to produce defects. For a representative structure of MoS_2, we carry out high-resolution transmission electron microscopy experiments and validate our theoretical predictions via observations of vacancy formation under exposure to a 80 keV electron beam. We further show that TMDs can be doped by filling the vacancies created by the electron beam with impurity atoms. Thereby, our results not only shed light on the radiation response of a system with reduced dimensionality, but also suggest new ways for engineering the electronic structure of TMDs.

PACS numbers: 31.15.es, 61.80.Fe, 61.72.Ff, 68.37.Og, 81.05.ue

Isolation of a single sheet of graphene in 2004 [1] indicated that strictly two-dimensional (2D) materials can exist at finite temperatures. Indeed, inorganic 2D systems such as individual hexagonal BN and transition metal dichalcogenide (TMD) layers were later on manufactured by mechanical [2, 3] and chemical [4, 5] exfoliation of their layered bulk counterparts, as well as by chemical vapor deposition [6, 7]. Recently, TMDs with a common structural formula MeX_2, where Me stands for transition metals (Mo, W, Ti, etc.) and X for chalcogens (S, Se, Te), have received considerable attention. These 2D materials are expected to have electronic properties varying from metals to wide-gap semiconductors, similar to their bulk counterparts [8, 9], and excellent mechanical characteristics [10]. The monolayer TMD materials have already shown a good potential in nanoelectronic [3, 11, 12] and photonic [4, 13, 14] applications.

Characterization of the *h*-BN [15–17] and TMD [5, 6, 18] samples has extensively been carried out using high-resolution transmission electron microscopy (HR-TEM). During imaging, however, energetic electrons in the TEM can give rise to production of defects due to ballistic displacements of atoms from the sample and beam-stimulated chemical etching [19], as studies on *h*-BN membranes also indicate [15–17, 20].

Contrary to *h*-BN, very little is known about the effects of electron irradiation on TMDs. So far, atomic defects have been observed via HR-TEM in WS_2 nanoribbons encapsulated inside carbon nanotubes at electron acceleration voltage of 60 kV [21] as well as at the edges of MoS_2 clusters under 80 kV irradiation [22], while no significant damage or amorphization was reported for MoS_2 sheets at 200 kV [18] – a surprising result taking into account the relatively low atomic mass of the S atom. Clearly, precise microscopic knowledge of defect production in TMDs under electron irradiation is highly desirable for assessing the effects of the beam on the samples. This knowledge would allow designing experimental conditions required to minimize damage, as well as developing beam-mediated post-synthesis doping techniques. Moreover, information on the displacement thresholds is important in the context of fundamental aspects of the interaction of beams of energetic particles with solids, as the reduced dimensionality may give rise to an irradiation response different from that in the bulk counterpart of the 2D material [23].

Here, by employing first-principles simulations, we study the behavior of a representative number of TMDs (21 compounds) under electron irradiation, and calculate the threshold energies for atomic displacements in each system, as well as displacement cross sections as functions of electron beam energy. In the case of MoS_2, we also carry out HR-TEM experiments and provide evidence of electron-irradiation-induced production of vacancies in this material. In addition – inspired by the recent advances in introducing impurities in *h*-BN monolayers [24, 25] – we discuss irradiation-mediated doping of TMD materials.

For all calculations in this work, we rely on the density-functional theory (DFT) with the PBE exchange-correlation functional [26] and the projector augmented wave formalism as implemented in the simulation package VASP [27, 28]. In order to obtain a comprehensive picture of the irradiation response of TMDs, we consider a large set of layered TMDs: MoX_2, WX_2, NbX_2, TaX_2, PtX_2, TiX_2, and VX_2 (where X=S, Se, or Te), which

have similar crystal structures.

We started our study by calculating the displacement threshold energy T_d (the minimum initial kinetic energy of the recoil atom) for sputtering an atom from the material. As in our previous simulations for graphene [29] and BN [20] monolayers, an initial velocity was assigned to the recoil atom (corresponding to instantaneous momentum transfer from the electron to the atom during the impact), then DFT molecular dynamics was used to model the time evolution of the system. In practice, the initial kinetic energy of the recoil atom was increased until it was high enough for the atom to be displaced from its lattice site without an immediate recombination with the resulting vacancy. The calculations were carried out using a 5×5 supercell of a MeX_2 monolayer. Test simulations for larger systems gave essentially the same results. The atomic structure of a MoS_2 layer and the simulation setup are shown in Fig. 1(a).

T_d required for displacing a chalcogen atom from the bottom layer of the sheet [cf. Fig. 1(a)] are presented in Fig. 2. In addition to the prototypical MoX_2 and WX_2, we also present results for TiS_2 and $TiTe_2$. As evident from the figure, $T_d \in [5, 7]$ eV for all studied compounds.

We also calculated the vacancy formation energies (E_f) for each of the compounds to see how it correlates with T_d. We defined E_f as:

$$E_f = E_{\rm vac} - (E_{\rm bulk} - \mu_{\rm X}), \qquad (1)$$

where $E_{\rm bulk}$ and $E_{\rm vac}$ are the energies of the pristine and vacancy containing supercells, respectively. The chemical potential $\mu_{\rm X}$ of the chalcogen species is taken as the energy of the isolated atom to enable a straightforward comparison with the results of dynamical simulations. E_f, with and without relaxation of the atomic structure of the layer, is also presented in Fig. 2.

In the non-relaxed case, the energetics is very similar for all materials, and – as can readily be noticed – the agreement between T_d and the *non-relaxed* E_f is striking. This is because during the sputtering of chalcogen atoms from the outermost layer, little energy is transmitted to the surrounding metal atoms due to sufficiently fast sputtering event and the rigidity of the structure. The energies for the relaxed geometries show a more intriguing behavior. Atomic relaxation for some systems evidently gives rise to a considerable drop in E_f, so that the similarity to T_d is lost. This drop quantifies the degree of structural relaxation around the vacancy, which is minor for MoS_2, see Fig. 1(b). The analysis of the electronic structure revealed an occupied bonding type vacancy state close to valence band maximum and an empty anti-bonding type state in the mid gap, which stabilizes the structure. For the occupied bonding defect state, the electronic charge is localized at the vacancy site, analogous to bulk MoS_2, where Mo atoms donate electrons to S atoms. This is true for all of the semiconducting materials: MoX_2, WX_2, and PtX_2. The rest of the considered materials are metals or semimetals, for which the bonding vacancy state may become unoccupied, which is reflected in larger relaxation and lower formation energies.

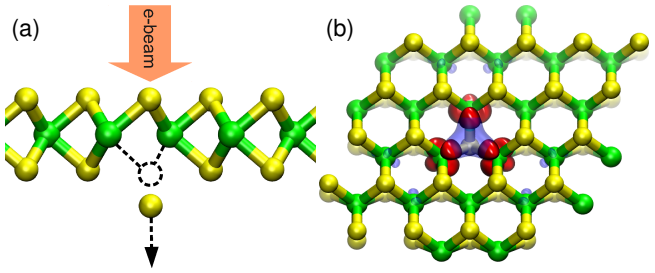

FIG. 1. (Color online) (a) The setup used in the dynamical DFT simulations of atom sputtering from TMDs under electron irradiation. Initial energy acquired due to the impact of an energetic electron was assigned to the recoil atom, then DFT molecular dynamics was used to model the evolution of the system. (b) MoS_2 sheet with an S vacancy. The charge densities of the occupied and unoccupied defect states are visualized by (blue) transparent and (red) solid isosurfaces, respectively.

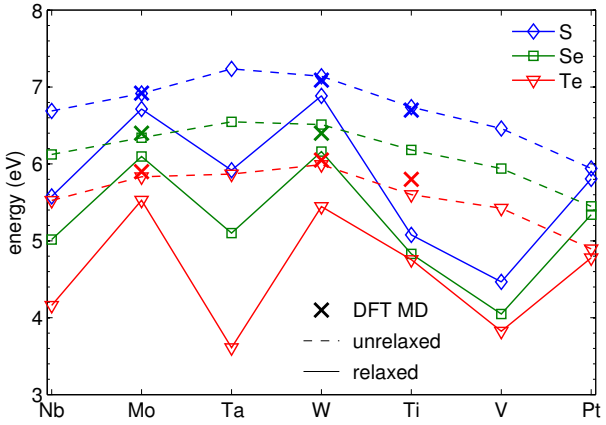

FIG. 2. (Color online) Displacement threshold energies T_d obtained from DFT molecular dynamics calculations (crosses) and formation energies of chalcogen vacancies with non-relaxed (dashed lines) and relaxed (solid lines) geometries in transition metal dichalcogenides MeX_2, X=S, Se, Te.

Knowing T_d, it is possible to estimate the electron threshold energy through the relativistic binary collision formula and the atom displacement cross section (for relatively light atoms) by using the McKinley-Feshbach formalism [30]. E_f for Se and Te compounds are smaller than in S compounds, but – due to the higher atomic mass – their creation through ballistic electron impacts requires significantly higher electron energies. In the case of MoS_2, $MoSe_2$, and $MoTe_2$, T_d of 6.9, 6.4 and 5.9 eV

correspond to electron energies of about 90, 190, and 270 keV, as calculated assuming a static lattice. For other compounds the required electron energies should be of similar magnitude, based on the close values of T_d in Fig. 2. An accurate estimation of the displacement cross section requires including the effects of lattice vibrations on the energy transferred from an electron to a target atom [31]. We calculated the cross sections for vacancy production as a function of electron energy for MoS_2, WS_2, and TiS_2 beyond the static lattice approximation, as shown in Fig. 3. We stress that the production of S vacancies for practically all TMDs is within the energies commonly used in TEM studies.

The displacement thresholds for chalcogen atoms in the (top) layer facing the beam proved to be considerably higher than for the bottom chalcogen layer, as the displaced atom is "stopped" by the other layers. However, after a vacancy is created in the bottom layer, the threshold energy for the top S atom in MoS_2 to be displaced and fill the vacancy is about 8.1 eV. This is similar in magnitude to the threshold for displacing S atom from the bottom layer (6.9 eV), and thus formation of vacancy columns should be possible even at 80 kV when lattice vibrations are accounted for. T_d for transition metals are even higher, since they are bonded to six neighbors and similarly stopped by the S layer. For instance, about 20 eV is required to displace Mo atom from its site in the MoS_2 lattice, which corresponds to electron energy of 560 keV. Naturally, under such conditions the S sublattice is quickly destroyed. Formation of transition metal vacancies is thus considered highly unlikely.

With regard to possible vacancy agglomeration under continuous irradiation, we found that creation of a vacancy does not alter the formation energy in the neighboring sites in the semiconducting TMDs. Thus, we do not expect accelerated formation of large vacancy clusters. In the same vein, however, it is worth noting that chalcogen atoms may also be sputtered fairly easily from the edges of nanostructures [21, 22]. For example, our calculations for a WS_2 ribbon show that the chalcogen atoms at the edge can have a displacement threshold as low as 4.2 eV, as compared to 7.0 eV away from the edge.

To check our theoretical results on irradiation-induced vacancy formation in MoS_2, we experimentally studied the evolution of a MoS_2 sheet under an 80 keV electron beam. First, free standing single layer MoS_2 samples were prepared by mechanical exfoliation of natural MoS_2 bulk crystals, followed by characterization via optical microscopy on a Si+90nm SiO_2 substrate and transfer to a perforated TEM support film (Quantifoil), similar to graphene samples [32]. The TEM grid was adhered to the SiO_2 surface by evaporating isopropanol on top of it. After this, the silica was etched with KOH. Aberration-corrected (AC) HRTEM imaging was carried out in an image-side Cs corrected FEI TITAN microscope at a primary beam energy of 80 keV. The contrast difference

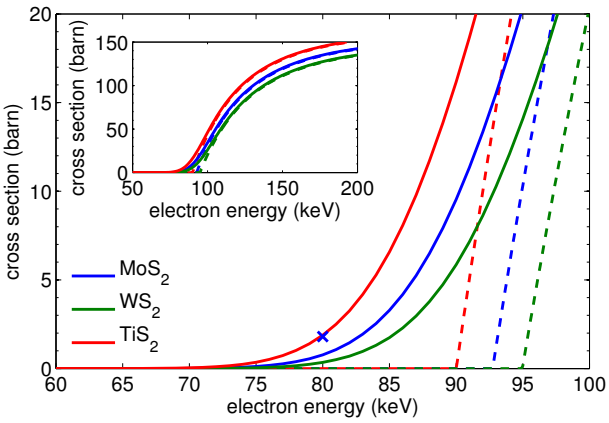

FIG. 3. (Color online) Cross section for sputtering a sulfur atom from MoS_2, WS_2, and TiS_2 sheets as calculated through the McKinley-Feshbach formalism and the dynamical values of the displacement thresholds. Dotted lines are the data for the static lattice, and solids lines are the results of calculations where lattice vibrations are taken into account assuming a Maxwell-Boltzmann velocity distribution. The cross denotes the experimentally determined cross section for MoS_2. The inset shows the same data for a larger range of electron energies.

between the Mo and S sublattice is clearly detectable in the AC-HRTEM images proving the single layer nature of the sheet (for a double layer the contrast would be identical as Mo is stacked above S). This is also confirmed in diffraction measurements, as successive diffraction spots from one $\{hkl\}$ family show different intensity, whereas for bi- and multilayers they are equal [18]. The analyzed intensity ratio of the $\{\bar{1}100\}$ diffraction spots was found to be 1.07.

During continuous imaging we found an increasing number of vacancy sites (exclusively on the S sublattice) accompanied by crack formation [see Fig. 4(a)] and lateral shrinkage of the membrane. Counting the actual number of sputtered atoms as in Ref. 31, the cross section for sputtering was found to be 1.8 barn, which is in a reasonable agreement with the calculated cross-section of 0.8 barn, taking into account that the theoretical estimates are very sensitive to inaccuracies in the parameters of the model (e.g., T_d and the velocity distribution) at energies below the static threshold.

In Fig. 4(d,e) we present simulated TEM images [33] for the single and double vacancies, respectively, based on atomic structures (Fig. 4(b,c)) obtained from the DFT calculations. Similar defects are observed in the experimental TEM images [Fig. 4(f)]. Different defects can clearly be distinguished by analyzing the (Michelson) contrast relative to the contrast of the Mo atoms in the pristine area. We find that the experimental (simulated) ratios are 0.9 (0.9) for a sulfur column, 0.5 (0.4) for the single- and 0.2 (0.2) for the double vacancy.

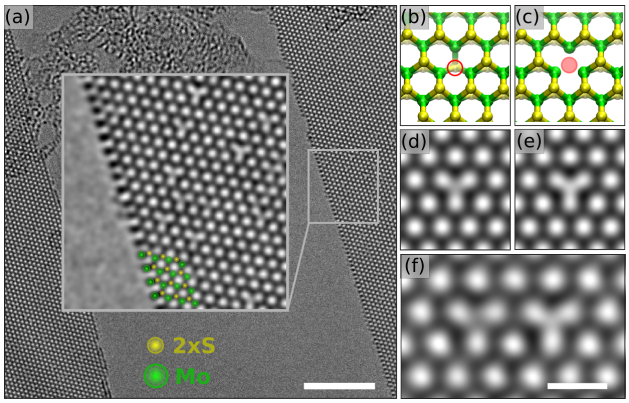

FIG. 4. (Color online) AC-HRTEM images of single-layer MoS_2. Atoms are dark and white spots correspond to the holes in the hexagonal structure. During continuous 80 keV electron irradiation a crack formed in the membrane (a). The edges are terminated with Mo atoms, as can be determined from the contrast in the inset. Also an increasing number of S vancancies is observed. Most of them are single vacancies but also double vacancies, where the top and bottom S atoms are removed, can be found. Structure models and corresponding HRTEM image simulations for both vacancy types are shown in (b, d) for the single- and (c, e) for the double vacancy. Experimental examples are shown in (f). To enhance the visibility of the defect, a Gaussian filter (0.7 Å FWHM) was applied to (d, e) and (f). Scale bars are 5 nm (a) and 5 Å (f).

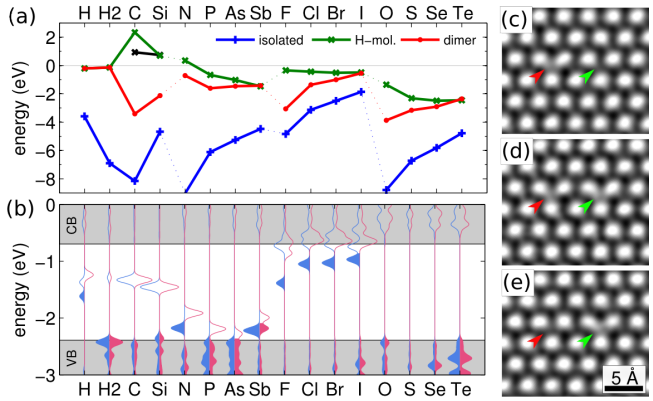

FIG. 5. (Color online) (a) Substitution energies of the impurity atoms in MoS_2 layer calculated for three different chemical potentials: isolated atoms (blue), diatomic molecules (red), and molecules with hydrogen (green). The solid phase reference is also given for carbon and silicon (black). (b) Respective local density of states of the impurity atoms, the spin-up and spin-down components. The gray areas denote the band edges of the MoS_2 layer. (c–e) Series of AC-HRTEM images demonstrating vacancy filling. The red arrow highlights an initial S vacancy that picks up an atom between (d) and (e), and the green arrow indicates an S atom that is sputtered away between (c) and (d), forming a single vacancy.

Having shown that vacancies can be created in TMDs under electron irradiation, we move on to study whether they could be consecutively filled with other atomic species deliberately introduced into the TEM chamber. We calculate the formation energy of substitutional defects in MoS_2 and consider donors F, Cl, Br, and I; acceptors, N, P, As, and Sb; double acceptors C and Si; hydrogen H and H_2; and isoelectronic species O, S, Se, and Te. The formation energies and the local density of states (LDOS) around the substitution site are shown in Fig. 5. We list the formation energies with three different chemical potentials of the substituted (impurity) species: the isolated atoms, diatomic molecules, or molecules with hydrogen (CH_4, SiH_4, NH_3, PH_3, AsH_3, HF, HCl, and HBr) where we set $\mu_{\mathrm{H}} = \frac{1}{2}E_{\mathrm{H}_2}$.

Due to the high formation energy of the vacancy, all substitutions are energetically favored with respect to the isolated atom. However, with respect to μ in the molecule, C, Si, and N substitution have positive formation energies. Obviously, even if the equilibrium energetics does not favor the formation of the substitutional defect, the substitution may still be achieved under electron beam, because molecules like N_2 or hydrocarbons will constantly break apart under the electron beam. Thus post-synthesis electron-mediated doping may also be realized in 2D TMDs, similar to BN sheets [24, 25]. The LDOS shows that N, P, As, and Sb behave as acceptors, whereas F, Cl, Br, and I are likely to be donors. C and Si have levels in the middle of the gap and the isoelectronic species like O, Se or Te do not produce any localized states, as expected.

Filling of the vacancies was also observed in the TEM images, as shown in the series of panels in Fig. 5(c–e). Although we could not identify the type of the impurity, this example proves that electron-beam-mediated doping is possible. Consequently, through control of atomic species in the TEM chamber and the choice of the electron energy, modification of the physical properties of TMDs via electron beam should be attainable.

To conclude, we calculated atom displacement threshold energies in a number of TMDs. These energies are a measure of the radiation hardness of the material, and serve as critical input parameters in the Kinchin-Pease and other semiclassical theories of defect production and ion stopping [23, 34]. Here we use them to calculate electron displacement energies and corresponding sputtering cross sections to quantitatively assess the amount of damage created in 2D TMD materials during a TEM experiment via knock-on processes. Observations of vacancies in our experimental AC-HRTEM images of single MoS_2 sheets validate our theoretical predictions. Finally, we observe filling of the vacancies and discuss the prospects for electron-beam mediated doping of TMDs.

We thank R. M. Nieminen for fruitful discussions. We acknowledge financial support by the University of

Helsinki Funds and the Academy of Finland through several projects. SK and UK are grateful to the German Research Foundation (DFG) and the State Baden Wuerttemberg in the frame of the SALVE project and to the DFG in the frame of the SFB-TRR21 project. We also thank CSC Finland for generous grants of computer time.

[1] K. S. Novoselov, A. K. Geim, S. V. Morozov, D. Jiang, Y. Zhang, S. V. Dubonos, I. V. Grigorieva, and A. A. Firsov, Science **306**, 666 (2004)
[2] K. S. Novoselov, D. Jiang, F. Schedin, T. J. Booth, V. Khotkevich, S. Morozov, and A. K. Geim, PNAS **102**, 10451 (2005)
[3] B. Radisavljevic, A. Radenovic, J. Brivio, V. Giacometti, and A. Kis, Nature Nanotech. **6**, 147 (2011)
[4] G. Eda, H. Yamaguchi, D. Voiry, T. Fujita, and M. Chen, Nano Letters **11**, 5111 (2011)
[5] J. N. Coleman, M. Lotya, A. O'Neill, S. D. Bergin, P. J. King, U. Khan, K. Young, A. Gaucher, S. De, R. J. Smith, I. V. Shvets, S. K. Arora, G. Stanton, H.-Y. Kim, K. Lee, G. T. Kim, G. S. Duesberg, T. Hallam, J. J. Boland, J. J. Wang, J. F. Donegan, J. C. Grunlan, G. Moriarty, A. Shmeliov, R. J. Nicholls, J. M. Perkins, E. M. Grieveson, K. Theuwissen, D. W. McComb, P. D. Nellist, and V. Nicolosi, Science **331**, 568 (2011)
[6] K. Kim, A. Hsu, X. Jia, S. Kim, Y. Shi, M. Hofmann, D. Nezich, J. Rodriguez-Nieva, M. Dresselhaus, T. Palacios, and J. Kong, Nano Letters **12**, 161 (2012)
[7] Y. Zhan, Z. Liu, S. Najmaei, P. M. Ajayan, and J. Lou, Small **8**, 966 (2012)
[8] J. Wilson and A. Yoffe, Adv. Phys. **18**, 193 (1969)
[9] C. Ataca, H. ahin, and S. Ciraci, J. Phys. Chem. C **116**, 8983 (2012)
[10] A. Castellanos-Gomez, M. Poot, G. a Steele, H. S. J. van der Zant, N. Agraït, and G. Rubio-Bollinger, Advanced Materials **24**, 772 (2012)
[11] H. Li, Z. Yin, Q. He, H. Li, X. Huang, G. Lu, D. W. H. Fam, A. I. Y. Tok, Q. Zhang, and H. Zhang, Small **8**, 63 (2012)
[12] I. Popov, G. Seifert, and D. Tománek, Phys. Rev. Lett. **108**, 156802 (2012)
[13] K. F. Mak, C. Lee, J. Hone, J. Shan, and T. F. Heinz, Phys. Rev. Lett. **105**, 136805 (2010)
[14] Z. Yin, H. Li, H. Li, L. Jiang, Y. Shi, Y. Sun, G. Lu, Q. Zhang, X. Chen, and H. Zhang, ACS Nano **6**, 74 (2012)
[15] J. C. Meyer, A. Chuvilin, G. Algara-Siller, J. Biskupek, and U. Kaiser, Nano Lett. **9**, 2683 (2009)
[16] C. Jin, F. Lin, K. Suenaga, and S. Iijima, Phys. Rev. Lett. **102**, 195505 (2009)
[17] J. C. Meyer, S. Kurasch, H. J. Park, V. Skakalova, D. Kunzel, A. Gross, A. Chuvilin, G. Algara-Siller, S. Roth, T. Iwasaki, U. Starke, J. H. Smet, and U. Kaiser, Nature Mater. **10**, 209 (2011)
[18] J. Brivio, D. T. L. Alexander, and A. Kis, Nano Letters **11**, 5148 (2011)
[19] K. Mølhave, S. B. Gudnason, A. T. Pedersen, C. H. Clausen, A. Horsewell, and P. Bøggild, Ultramicroscopy **108**, 52 (2007)
[20] J. Kotakoski, C. H. Jin, O. Lehtinen, K. Suenaga, and A. V. Krasheninnikov, Phys. Rev. B **82**, 113404 (2010)
[21] Z. Liu, K. Suenaga, Z. Wang, Z. Shi, E. Okunishi, and S. Iijima, Nature Comm. **2**, 213 (2011)
[22] L. P. Hansen, Q. M. Ramasse, C. Kisielowski, M. Brorson, E. Johnson, H. Topsøe, and S. Helveg, Angew. Chem. Int. Ed. **50**, 10153 (2011)
[23] A. V. Krasheninnikov and K. Nordlund, J. Appl. Phys. **107**, 071301 (2010)
[24] X. Wei, M. Wang, Y. Bando, and D. Golberg, ACS Nano **5**, 29162922 (2011)
[25] O. L. Krivanek, M. F. Chisholm, V. Nicolosi, T. J. Pennycook, G. J. Corbin, N. Dellby, M. F. Murfitt, C. S. Own, Z. S. Szilagyi, M. P. Oxley, S. T. Pantelides, and S. J. Pennycook, Nature **464**, 571 (2010)
[26] J. P. Perdew, K. Burke, and M. Ernzerhof, Phys. Rev. Lett. **77**, 3865 (1996)
[27] G. Kresse and J. Hafner, Phys. Rev. B **47**, 558 (1993)
[28] G. Kresse and J. Furthmüller, Comput. Mat. Sci. **6**, 15 (1996)
[29] J. Kotakoski, D. Santos-Cottin, and A. V. Krasheninnikov, ACS Nano **6**, 671 (2011)
[30] W. A. McKinley and H. Feshbach, Phys. Rev. **74**, 1759 (1948)
[31] J. C. Meyer, F. Eder, S. Kurasch, V. Skakalova, J. Kotakoski, H. Park, S. Roth, A. Chuvilin, S. Eyhusen, G. Benner, A. V. Krasheninnikov, and U. Kaiser, Phys. Rev.Lett. **108**, 196102 (2012)
[32] J. C. Meyer, C. O. Girit, M. F. Crommie, and a. Zettl, Applied Physics Letters **92**, 123110 (2008)
[33] C. Koch, *Determination of core structure periodicity and point defect density along dislocations*, Ph.D. thesis, Arizona State University (2002)
[34] G. H. Kinchin and R. S. Pease, Rep. Prog. Phys. **18**, 1 (1955)